Synthesis, Structure, and Molecular Orbital Calculation of the Bicapped Triangular Molybdenum Cluster Complex $[Mo_3S_5(PMe_3)_6]$

Kiyoshi Tsuge, Hideo Imoto, and Taro Saito*

Department of Chemistry, School of Science, The University of Tokyo, Hongo, Tokyo 113, Japan

Received May 20, 1994[⊗]

Treatment of the sulfur monocapped molybdenum trinuclear cluster $(NH_4)_2[Mo_3S_{13}]$ with excess trimethylphosphine affords the sulfur bicapped molybdenum trinuclear cluster complex $[Mo_3(\mu_3\text{-}S)_2(\mu_2\text{-}S)_3(PMe_3)_6]$. This compound crystallizes in the rhombohedral space group $R\bar{3}c$ with $a = 11.112(1)$ Å, $c = 53.507(10)$ Å, $V = 5722(1)$ Å, $Z = 6$, $R = 0.043$, and $R_w = 0.026$. The Mo_3 triangle is equilateral with the Mo−Mo distance 2.714(1) Å. Calculations by the DV−Xα method on this compound show that the structural difference from an isoelectronic cluster anion $[Mo_3S_2Cl_9]^{3-}$ is caused by the reversal of the HOMO and LUMO. Calculated populations and a qualitative molecular orbital discussion reveal that this reversal is due to the π antibonding interaction between the metal atoms and bridging ligands. Construction of qualitative MOs clarifies the effect of the M−L π interaction on the MOs derived from metal t_{2g} orbitals in the $M_3X_5L_6$-type and $M_3X_4L_9$-type clusters where metal atoms are in the octahedral coordination.

Introduction

Many cluster complexes with the Mo_3X_4 core of a Mo_3 triangle capped by an X atom have been prepared with various ligand combinations (X = O, S, Cl, etc.).[1-6] The number of skeletal electrons is 6 for most of the Mo_3X_4 clusters. When the trinuclear clusters have six electrons, they are electron precise for three Mo−Mo bonds and stable.[3,7,8] Eight-electron clusters have also been synthesized with halogen bridging ligands.[9-11] The MO calculations on these clusters have revealed that the stability is due to the π interaction between molybdenum d orbitals and bridging chlorine 3p orbitals.[8,12,13]

In contrast to the abundance of the Mo_3X_4-type clusters, there are only a few examples of Mo_3X_5-type clusters in which the Mo_3 triangle is capped on both sides.[2,14,15] The cluster anion $[Mo_3S_2Cl_9]^{3-}$ is the first example of a sulfur-bicapped molybdenum trinuclear cluster complex.[16] The cluster anion $[Mo_3S_2Cl_9]^{3-}$ has an isosceles Mo_3 triangle with eight skeletal electrons. The relation between the molecular and electronic structures of this compound was discussed on the basis of MO calculations.[15] We have synthesized the second example of a sulfur-bicapped molybdenum trinuclear cluster complex $[Mo_3S_5(PMe_3)_6]$ by treating $(NH_3)_2[Mo_3S_{13}]$ with excess PMe_3.[17] Though the number of skeletal electrons is also eight, the Mo_3 triangle is equilateral. The preliminary MO calculations have suggested that this structural difference is due to the effect of the π interaction between the sulfur and molybdenum atoms.[17] In this paper, we will describe the relation between the electronic and molecular structures of $[Mo_3S_5(PMe_3)_6]$ with the details of the synthesis, structural determination, and electronic structure calculations.

Experimental Section

Synthesis of $[Mo_3S_5(PMe_3)_6]$. All manipulations were carried out under an atmosphere of nitrogen or argon. $(NH_4)_2[Mo_3S_{13}]$ was prepared by the literature procedure.[18] THF was distilled under argon from sodium/benzophenone.

A suspension of $(NH_4)_2[Mo_3S_{13}]$ (0.5 g, 0.68 mmol) in THF (25 mL) was treated with PMe_3 (14 mmol, Aldrich) in THF. After being stirred for 10−15 min, the suspension became a black solution which was allowed to stand at room temperature. Black single crystals appeared after 1−2 days. Yield: 0.16 g (25%). Anal. Calcd for $C_{18}H_{54}Mo_3P_6S_5$: C, 23.89; H, 5.97. Found: C, 23.47; H, 5.82. IR/cm^{-1}: 368, 340; the peaks above 400 cm^{-1} are due to PMe_3. ^{1}H NMR ($CDCl_3$): δ 1.37 (broad singlet, half-width 20 Hz). ^{31}P{^{1}H} NMR ($CDCl_3$): δ 30.4 (85% H_3PO_4). XPS: Mo $3d_{5/2}$, −228.6 eV; Mo $3d_{3/2}$, −231.7 eV; S 2p, −161.5 eV; P 2p, −131.2 eV.

Structure Determination of $[Mo_3S_5(PMe_3)_6]$. A rhombohedral single crystal (0.2 × 0.2 × 0.2 mm^3) sealed in a capillary under an argon atmosphere was used for X-ray data collection. Crystallographic data and the parameters associated with data collection and structure refinement are given in Table 1 and the supporting information (formerly known as supplementary material). All X-ray measurements were made on a Rigaku AFC-5R diffractometer with Mo Kα radiation monochromatized with graphite. No decay of the diffraction was

[⊗] Abstract published in *Advance ACS Abstracts*, June 1, 1995.

(1) (a) Shibahara, T. *Adv. Inorg. Chem.* **1991**, *37*, 143. (b) Shibahara, T. *Coord. Chem. Rev.* **1993**, *123*, 73 and references therein.
(2) Cotton, F. A. *Polyhedron* **1986**, *5*, 3.
(3) Müller, A.; Jostes, R.; Cotton, F. A. *Angew. Chem., Int. Ed. Engl.* **1980**, *19*, 875.
(4) (a) Shibahara, T.; Yamasaki, M.; Watase, T.; Ichimura, A. *Inorg. Chem.* **1994**, *33*, 292. (b) Shibahara, T.; Yamasaki, M.; Sakane, G.; Minami, K.; Yabuki, T.; Ichimura, A. *Inorg. Chem.* **1992**, *31*, 640.
(5) Cotton, F. A.; Dori, Z.; Llusar, R.; Schwotzer, W. *J. Am. Chem. Soc.* **1985**, *107*, 6734.
(6) Shang, M.; Huang, J.; Lu, J. *Acta Crystallogr.* **1984**, *C40*, 759.
(7) Cotton, F. A.; Haas, T. E. *Inorg. Chem.* **1964**, *3*, 10.
(8) Bursten, B. E.; Cotton, F. A.; Hall, M. B.; Najjar, R. C. *Inorg. Chem.* **1982**, *21*, 302.
(9) Cotton, F. A.; Shang, M.; Sun, Z. S. *J. Am. Chem. Soc.* **1991**, *113*, 6917.
(10) Cotton, F. A.; Shang, M.; Sun, Z. S. *J. Am. Chem. Soc.* **1991**, *113*, 3007.
(11) Birnbaum, A.; Cotton, F. A.; Dori, Z.; Kapon, M.; Marler, D.; Reisner, G. M.; Schwotzer, W. *J. Am. Chem. Soc.* **1985**, *107*, 2405.
(12) (a) Cheng, W.-D.; Zhang, Q.-E.; Huang, J.-S.; Lu, J.-X. *Polyhedron* **1989**, *8*, 2785. (b) Cheng, W.-D.; Zhang, Q.-E.; Huang, J.-S.; Lu, J.-X. *Polyhedron* **1990**, *9*, 1625.
(13) Cotton, F. A.; Feng, X. *Inorg. Chem.* **1991**, *30*, 3666.
(14) Chisholm, M. H.; Folting, K.; Huffman, J. C.; Kirkpatrick, C. C. *Inorg. Chem.* **1984**, *23*, 1021.
(15) Jiang, Y.; Tang, A.; Hoffmann, R.; Huang, J.; Lu, J. *Organometallics* **185**, *4*, 27.
(16) Huang, J.; Shang, M.; Lui, S.; Lu, J. *Sci. Sin., Ser. B (Engl. Transl.)* **1982**, *25*, 1270.
(17) Tsuge, K.; Yajima, S.; Imoto, H.; Saito, T. *J. Am. Chem. Soc.* **1992**, *114*, 7910.
(18) (a) Müller, A.; Krickemeyer, E. *Inorg. Synth.* **1990**, *27*, 47. (b) Müller, A.; Bhattacharyya, R. G.; Pfefferkorn, B. *Chem. Ber.* **1979**, *112*, 778.

0020-1669/95/1334-3404$09.00/0

Table 1. Crystallographic Data for $[Mo_3S_5(PMe_3)_6]$

formula	$C_{18}H_{54}Mo_3P_6S_5$
fw	904.6
space group	$R\bar{3}c$
a, Å	11.112(1)
c, Å	53.507(10)
cell vol, Å^3	5722(1)
Z	6
$\varrho_{calcd.}$, g cm^{-3}	1.575
temp, K	297
2θ limit, deg	$5 < 2\theta < 60$
no. of measd reflns	4019
no. of unique reflns	2006
no. of obsd reflections	1534
criterion for obsd refln	$\|F_o\| > 3\sigma(\|F_o\|)$
linear abs coeff μ, cm^{-1}	14.7
no. of variable params	51
$R(F)$,[a] $R_w(F)$[b]	0.043, 0.026

[a] $R(F) = \sum(|F_o| - |F_c|)/\sum|F_o|$. [b] $R_w(F) = (\sum(w|F_o| - |F_c|)^2/\sum w|F_o|^2)^{1/2}$ with $w = 1/\sigma^2(F_o)$.

Table 2. Positional and Equivalent Isotropic Thermal Parameters for $[Mo_3S_5(PMe_3)_6]$

atom	x	y	z	U_{iso}, Å^2
Mo	−0.14102(2)	0	0.25	0.0342(1)
S1	0	0	0.28449(2)	0.0419(4)
S2	0.24786(7)	0	0.25	0.0464(5)
P	−0.29602(7)	0.01042(8)	0.28362(1)	0.0600(4)
C1	−0.3760(3)	0.1168(3)	0.27816(6)	0.135(3)
C2	−0.4346(4)	−0.1462(3)	0.29457(8)	0.210(3)
C3	−0.2048(3)	0.1011(4)	0.31175(5)	0.137(3)

Table 3. Selected Bond Distances (Å) and Bond Angles (deg)[a]

Mo−Mo′	2.7142(4)	S1−Mo−S2′	87.055(8)
Mo−S1	2.4211(8)	S1−Mo−S2″	87.055(8)
Mo−S2′	2.3928(6)	S1−Mo−P	85.04(2)
Mo−P	2.5328(7)	S2′−Mo−P	90.94(1)
Mo′−Mo−Mo″	60.00	S2′−Mo−P‴	95.47(1)
S1−Mo−P‴	175.08(2)	P−Mo−P‴	90.68(3)
S2′−Mo−S2″	170.90(2)	Mo−S1−Mo′	68.18(2)
S1−Mo−S1‴	99.33(3)	Mo′−S2−Mo″	69.10(2)

[a] Symmetry codes: ′ = $-y, x-y, z$; ″ = $-x+y, -x, z$; ‴ = $x-y, -y, -z+{}^1/_2$.

observed. An empirical absorption correction was applied (relative transmission coefficient 0.958−0.996). The observed systematic absences ($-h+k+l = 3n$, $l = 2n$ for $00l$) limited the possible space groups to $R3c$ and $R\bar{3}c$. We assumed $R\bar{3}c$ and successfully solved the structure. The position of the molybdenum atom was determined by direct methods (SHELXS-86),[19] and other non-hydrogen atoms were located in successive Fourier maps (SHELXS-76).[20] Methyl hydrogen atoms were fixed at the positions where the dihedral angle H−C−P−Mo was $60 + 120n°$. At the final state of the refinements, an empirical extinction correction proportional to the observed intensities was included. The structure was refined by full-matrix least-squares analysis (ANYBLK)[21] to residuals of $R = 0.043$, and $R_w = 0.026$ for the 1534 reflections with $F > 3\sigma(F)$. Positional parameters are given in Table 2; selected bond lengths and bond angles are given in Table 3.

Calculations. The molecular orbital were calculated by the DV−Xα method with the SCC approximation.[22−25] All calculations were performed on a Mips RS3230 computer. The exchange parameter α was taken to be 0.70 in all calculations. Numerical atomic orbitals from atomic Hartree−Fock−Slater calculations were used as basis functions. Atomic orbitals 1s to 5p were used for Mo, 1s to 3p for P, S, and Cl, and 1s for H. The SCF equations were converged by a self-consistent charge procedure[23,24] with the convergence criterion that the maximum change in the population between two consecutive iterations was less than 10^{-4}. The population analysis was performed with both Mulliken and Löwdin methods.[26] Because Mulliken population analysis gave negative populations for higher AOs, we used the Löwdin method, but differences of the energy levels obtained by the two methods were trivial. The number of sampling points was 200 000 for both $[Mo_3S_5(PH_3)_6]$ and $[Mo_3S_2Cl_9]^{3-}$. The geometries of model compounds were taken from the averaged values of each compound, and D_{3h} symmetry was assumed. The bond distances and angle in the model cluster $[Mo_3S_5(PH_3)_6]$ were Mo−Mo 2.714 Å, Mo−(μ_3-S) 2.421 Å, Mo−(μ_2-S) 2.393 Å, Mo−P 2.533 Å, and P−Mo−P 90.7°. The P−H distances of the phosphine ligands were set at 1.40 Å, and the angles Mo−P−H, at 114.63°. The dihedral angle (μ_3-S)−Mo−P−H was assumed to be 0°. The bond distances and angle in $[Mo_3S_2Cl_9]^{3-}$ were Mo−Mo 2.617 Å, Mo−S 2.375 Å, Mo−(μ_2-Cl) 2.467 Å, Mo−Cl(terminal) 2.447 Å, and Cl(terminal)−Mo−Cl(terminal) 90.0°.

The transition energies were calculated by the transition-state method with 200 000 sampling points. The number of sampling points used for the calculation of the oscillation strength was 600 000.

Results and Discussion

Synthesis. Many reactions of $(NH_4)_2[Mo_3S_{13}]$ with nucleophilic reagents have been reported, in which the terminal disulfido ligands are replaced without change of the oxidation states of molybdenum.[27,28] In this reaction of $(NH_4)_2[Mo_3S_{13}]$ with trimethylphosphine, the oxidation state of molybdenum is reduced from +4 to +3.33. Because the oxidation state of molybdenum remains the same on the change of μ_2-S_2 to μ_2-S, the molybdenum atoms must be reduced by the removal of the terminal disulfido ligand according to the scheme

$$Mo^m{-}S_2^{2-} \xrightarrow[-SPMe_3]{} Mo^m{-}S^{2-} \xrightarrow[-SPMe_3]{} Mo^{m-2}$$

A probable overall chemical equation can be formulated as

$$(NH_4)_2[Mo_3S_{13}] + 13PMe_3 \rightarrow [Mo_3S_5(PMe_3)_6] + 7SPMe_3 + (NH_4)_2S$$

For the preparation of $[Mo_3S_5(PMe_3)_6]$, excess trimethylphosphine ($PMe_3/Mo_3 > 20$) was necessary. Excess trimethylphosphine seems to prevent condensation of the Mo_3 cores to form larger clusters. If a smaller amount of trimethylphosphine is reacted with $(NH_4)_2[Mo_3S_{13}]$, a tetranuclear molybdenum cluster complex $[Mo_4S_6(SH)_2(PMe_3)_6]$ is mainly obtained.[29] The oxidation state of molybdenum atoms in the tetranuclear

(19) Sheldrick, G. M. SHELXS-86, Program for Crystal Structure Determination. University of Göttingen, Federal Republic of Germany, 1986.
(20) Sheldrick, G. M. SHELXS-76, Program for Crystal Structure Determination. University of Cambridge, U.K., 1976.
(21) Imoto, H.; Hayakawa, S.; Morita, N.; Saito, T. *Inorg. Chem.* **1990**, *29*, 2007.
(22) Slater, C. J. *The Calculation of Molecular Orbitals*; John Wiley & Sons: New York, 1979; p 52.
(23) Averill, F. W.; Ellis, D. E. *J. Chem. Phys.* **1973**, *59*, 6412 and reference therein.
(24) Rosén, A.; Ellis, D. E.; Adachi, H.; Averill, F. W. *J. Chem. Phys.* **1976**, *65*, 3629.
(25) (a) Adachi, H.; Tsukada, M.; Satoko, C. *J. Phys. Soc. Jpn.* **1978**, *45*, 875. (b) Satoko, C.; Tsukada, M.; Adachi, H. *J. Phys. Soc. Jpn.* **1978**, *45*, 1333. (c) Adachi, H.; Shiokawa, S.; Tsukada, M.; Satoko, C.; Sugano, S. *J. Phys. Soc. Jpn.* **1979**, *47*, 1528.
(26) (a) Löwdin, P.-O. *Adv. Quantum Chem.* **1970**, *5*, 185. (b) Szabo, A.; Ostlund, N. S.; *Modern Quantum Chemistry*, Revised 1st ed.; McGraw-Hill: New York, 1989; p 149.
(27) (a) Zimmermann, H.; Hegetschweiler, K.; Keller, T.; Gramlich, V.; Schmalle, H. W.; Petter, W.; Schneider, W. *Inorg. Chem.* **1991**, *30*, 4336. (b) Fedin, V. P.; Sokolov, M. N.; Mironov, Y. V.; Kolesov, B. A.; Tkachev, S. V.; Fedrov, V. Y. *Inorg. Chim. Acta* **1990**, *167*, 39. (c) Hegetschweiler, K.; Keller, T.; Zimmermann, H.; Schneider, W.; Schmalle, H.; Dubler, E. *Inorg. Chim. Acta* **1990**, *169*, 235.
(28) (a) Müller, A.; Reinsch, U. *Angew. Chem., Int. Ed. Engl.* **1980**, *19*, 72. (b) Halbert, T. R.; McGauley, K.; Pan, W.-H.; Czernuszewicz, R. S.; Stiefel, E. I. *J. Am. Chem. Soc.* **1984**, *106*, 1849. (c) Cotton, F. A.; Llusar, R.; Marler, D. O.; Schwotzer, W.; Dori, Z. *Inorg. Chim. Acta* **1985**, *102*, L25.
(29) Tsuge, K.; Imoto, H.; Saito, T. *Inorg. Chem.* **1992**, *31*, 4715.

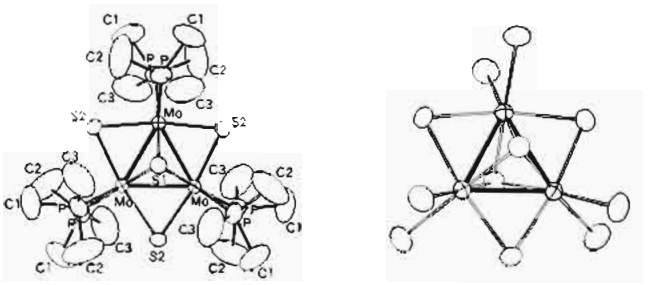

Figure 1. ORTEP drawings of $[Mo_3S_5(PMe_3)_6]$: (a) viewed down the D_3 axis; (b) viewed from the angle corresponding to the model in Figure 2a. Methyl groups are omitted for clarity. The thermal ellipsoids are drawn at the 50% level in both (a) and (b).

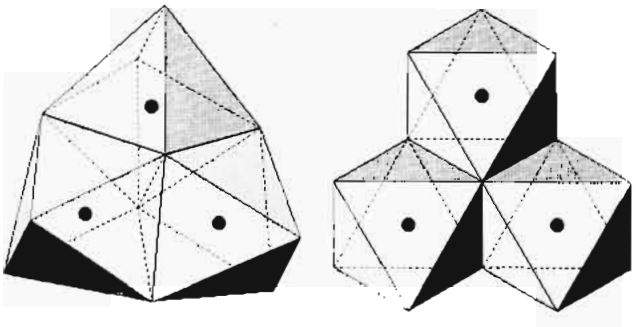

Figure 2. The octahedral models: (a) three face-linked octahedra ($M_3X_5L_6$); (b) three edge-linked octahedra ($M_3X_4L_6$).

complex is +3.5. Accordingly, reduction of the molybdenum occurs in both reactions of $(NH_4)_2[Mo_3S_{13}]$ with trimethylphosphine.

Structure. ORTEP drawing of $[Mo_3S_5(PMe_3)_6]$ are shown in Figure 1. The molecule of $[Mo_3S_5(PMe_3)_6]$ has an equilateral triangle of molybdenum atoms capped by two sulfur atoms and bridged by three sulfur atoms. There are six trimethylphosphines at the terminal positions of the Mo_3 triangle. The space group $R\bar{3}c$ imposes D_3 symmetry on the molecule. The 3-fold axis passes through two capping sulfur atoms, and the 2-fold axis passes through a molybdenum atom and a bridging sulfur atom. The positions of phosphorus atoms are rotated by 7° around the 2-fold axis from the D_{3h} positions. The packing of the molecules is close to fcc. The value of c/a is 4.82 for this crystal and is 4.90 for the idealized fcc.

Each molybdenum atom is octahedrally coordinated by two capping sulfur atoms, two bridging sulfur atoms, and two phosphorus atoms. The three coordination octahedra share faces with others as shown in Figure 2a. In this arrangement, the dihedral angle of two neighboring faces of the octahedra is 120°, but this angle in the regular octahedron is 109.47°. Therefore, the octahedra are distorted and the angle (μ_2-S)−Mo−(μ_2-S) is changed from 180 to 170.9°.

The Mo−Mo distance in $[Mo_3S_5(PMe_3)_6]$ is 2.71 Å, which is shorter than that in compounds of the Mo_3S_4 type (2.73−2.83 Å).[1] On the other hand, the Mo−S distances are longer: Mo−(μ_3-S) 2.42 Å and Mo−(μ_2-S) 2.39 Å in $[Mo_3S_5(PMe_3)_6]$ vs Mo−(μ_3-S) 2.31−2.36 Å and Mo−(μ_2-S) 2.28−2.34 Å in Mo_3S_4-type compounds.[1] These differences in bond distances are attributed to the difference in the oxidation states of molybdenum.

Calculations. We have carried out a calculation on a model compound $[Mo_3S_5(PH_3)_6]$ assuming D_{3h} symmetry by the DV−Xα method. The orbital energies and populations near the HOMO level are shown in Figure 3. Contour diagrams for several important wave functions are shown in Figure 4. The HOMO is $4a_1''$ which has 91% Mo 4d character and shows weak metal−metal antibonding interaction. The next HOMO (32e′) and the $27a_1'$ orbital have large Mo 4d orbital characters with metal−metal bonding interactions, and the metal−metal bonds are primarily made of these two MOs. Near these metal−metal bonding orbitals, there are $18a_2''$ and 18e″ orbitals which are the MOs of bridging μ_2-S lone pairs. The $18a_2''$ orbital has 82% μ_2-S 3p character, and the contribution of other AOs is small because of its a_2'' symmetry. On the other hand, the 18e″ orbital has 20% Mo 4d character and is stabilized by metal−ligand π interaction. The LUMO 19e″ is mainly composed of Mo 4d and μ_2-S 3p. This MO has weak metal−metal bonding character but is destabilized by metal−ligand interaction. The π interaction between molybdenum 4d orbitals and bridging sulfur 3p orbitals stabilizes the 18e″ orbital and destabilizes the 19e″.

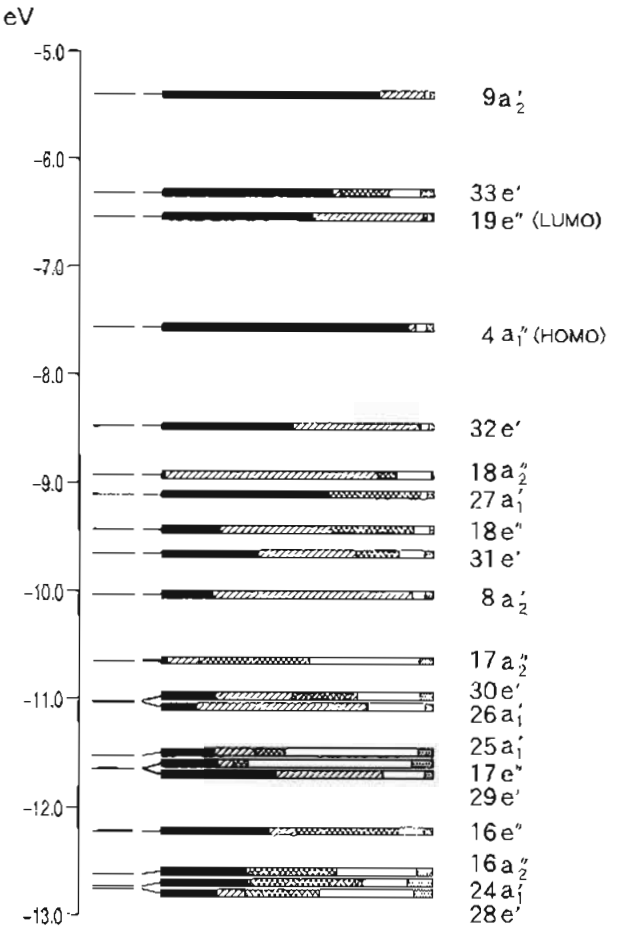

Figure 3. Orbital levels and populations of $[Mo_3S_5(PH_3)_6]$. Short horizontal lines show the energies of the levels. The strips show the AO compositions of each MO: black, 4d5s5p(Mo); hatched, 3s3p(μ_2-S); cross-hatched, 3s3p(μ_3-S); white, 3s3p(P); dotted, 1s(H).

Electronic Absorption Spectrum. The molybdenum trinuclear cluster complexes have characteristic electronic absorption spectra, which have been used to characterize the complexes.[5,9] The interpretation of the observed electronic spectra with MO calculations has been attempted for a few compounds. The spectra were, however, interpreted only through the calculated transition energies since the oscillation strengths were not evaluated.[30,31] As shown in Figure 5, the electronic spectrum

(30) Chisholm, M. H.; Cotton, F. A.; Fang, A.; Kober, E. M. *Inorg. Chem.* **1984**, *23*, 749.

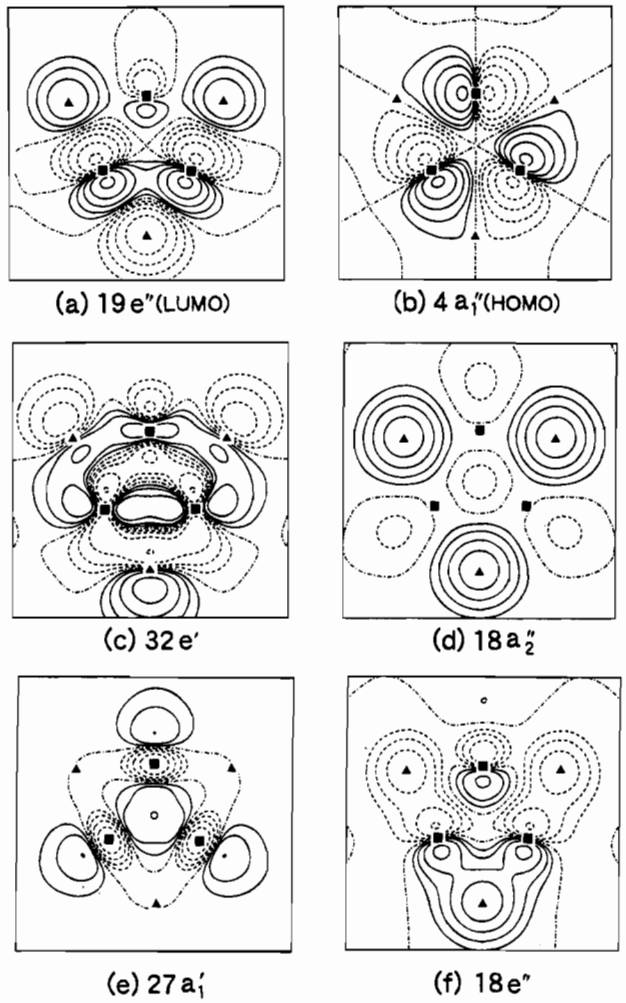

Figure 4. Contour diagrams on the plane 0.5 Å above the Mo_3 triangle: (a) 19e″ (LUMO); (b) $4a_1$″(HOMO); (c) 32e′; (d) $18a_2$″; (e) $27a_1$′; (f) 18e″. The symbols ■ and ▲ show the positions of molybdenums and bridging sulfurs, respectively. Dashed lines indicate negative contour values.

Table 4. Calculated Transitions of $[Mo_3S_5(PH_3)_6]$

	energy, eV	assignt	nature
A	1.07	$4a_1'' \rightarrow 19e''$	from Mo−Mo π antibonding to Mo−Mo π bonding
B	2.24	$32e' \rightarrow 33e'$	from Mo−Mo bonding to Mo−Mo antibonding
C	2.47	$18a_2'' \rightarrow 19e''$	from μ_2-S lone pair orbital to Mo−Mo π bonding
D	2.81	$27a_1' \rightarrow 33e'$	from Mo−Mo bonding to Mo−Mo antibonding

of $[Mo_3S_5(PMe_3)_6]$ shows bands ($\epsilon \sim 10^3$) in the visible region higher than 2 eV (1.6×10^4 cm^{-1}) and a characteristic band in the near-infrared region (~0.8 eV (6.5×10^3 cm^{-1})) where six-electron molybdenum trinuclear cluster complexes have no absorption. To assign the absorption bands, we have calculated the transition energies and oscillation strengths of the model complex $[Mo_3S_5(PH_3)_6]$. The results are shown in Table 4 and Figure 5. The calculated transition energies due to LMCT and MMCT are in the region higher than 2 eV, and the transition between the HOMO and the LUMO is near 1 eV. Comparing the results of the calculation with the observed spectrum, we assign the observed low-energy absorption to the transition from the HOMO to the LUMO. As described in the calculation section, the HOMO is weakly metal−metal antibonding in $[Mo_3S_5(PH_3)_6]$. Therefore, the HOMO−LUMO gap is smaller than that for six-electron trinuclear clusters and the complex has the characteristic absorption in the near-infrared region.

Comparison with $[Mo_3S_2Cl_9]^{3-}$. Another sulfur-bicapped molybdenum cluster complex $[Mo_3S_2Cl_9]^{3-}$ has the same ligand arrangement and the same number of skeletal electrons as $[Mo_3S_5(PMe_3)_6]$. However, the Mo_3 triangle of $[Mo_3S_2Cl_9]^{3-}$ is not equilateral and the Mo−Mo distances are 2.653, 2.641, and 2.556 Å.[16] In order to explain this structural difference, we have performed DV−Xα calculations on a model cluster of $[Mo_3S_2Cl_9]^{3-}$ assuming D_{3h} symmetry. The orbital energies of $[Mo_3S_2Cl_9]^{3-}$ are shown in Figure 6. The HOMO is the 19e″ and the LUMO is the $4a_1$″. Since the HOMO is a half-filled degenerate orbital, the Mo_3 triangle in $[Mo_3S_2Cl_9]^{3-}$ is liable to distortion by the Jahn−Teller effect. These results obtained by the present DV−Xα method are in good agreement with the previous EHMO calculations.[15]

The populations in Figures 3 and 6 indicate that $4a_1$″, the HOMO, of $[Mo_3S_5(PH_3)_6]$ corresponds to $4a_1$″, the LUMO, of $[Mo_3S_2Cl_9]^{3-}$. Similarly, the 19e″ orbitals, the LUMO in $[Mo_3S_5(PH_3)_6]$ and the HOMO in $[Mo_3S_2Cl_9]^{3-}$, correspond to each other. In the two compounds, therefore, the order of the two orbitals is reversed. The interaction between AOs is of the π type in the $4a_1$″ and 19e″ orbitals because an MO with the ″ symmetry notation is antisymmetrical about the Mo_3 plane. The $4a_1$″ orbitals of both clusters are localized almost on the molybdenum atoms and have M−M π antibonding character as indicated in the contour diagram (Figure 4). Because the combinations of the p orbitals of the bridging ligands do not produce the a_1″-type orbital, the $4a_1$″ orbitals are not affected by the M−L interaction. The 19e″ orbitals have M−M π bonding character and M−L π antibonding character (Figure 4). Since $4a_1$″ is destabilized by the M−M π antibonding interaction, the 19e″ orbital has a lower energy and becomes the HOMO when the M−M π bonding interaction is stronger than the M−L π antibonding interaction in 19e″. However, if the M−L π antibonding interaction is strong, the 19e″ orbital is destabilized and when the 19e″ has a higher energy than the $4a_1$″ orbital, the $4a_1$″ orbital becomes the HOMO. The HOMO and LUMO of these clusters are determined by the π antibonding interaction between molybdenum atoms and bridging ligands. The level order in the $[Mo_3S_2Cl_9]^{3-}$ cluster is the former weak π interaction case, and the level order in the $[Mo_3S_5(PH_3)_6]$ cluster is the latter strong π interaction case. The populations reflect the differences in the interactions. The 19e″ orbital of $[Mo_3S_2Cl_9]^{3-}$ has 66% Mo 4d character and 10% Cl 3p character while the 19e″ orbital of $[Mo_3S_5(PH_3)_6]$ has 55% Mo 4d character and 39% μ_2-S 3p character. The average Mo−Mo bond lengths reflect the differences in bonding properties of the HOMOs. In $[Mo_3S_2Cl_9]^{3-}$, having the M−M bonding HOMO, the average Mo−Mo bond length is 2.62 Å, which is 0.09 Å shorter than that for $[Mo_3S_5(PMe_3)_6]$.

The Metal−Ligand π Interaction in Mo_3 Clusters. As discussed above, in the $Mo_3(\mu_3\text{-}X)_2(\mu_2\text{-}X)_3L_6$ (=Mo_3X_5) type cluster complexes, the interactions between the molybdenum d orbitals and the lone pairs of bridging ligands determine the order of the energy levels near the HOMO and consequently affect the structure. Metal−ligand interactions are also important in the monocapped $Mo_3(\mu_3\text{-}X)(\mu_2\text{-}X)_3L_9$ (=Mo_3X_4) type cluster complexes.[12,13] Both types of clusters have the structures

(31) Müller, A.; Wittneben, V.; Krickmeyer, E.; Bögge, H.; Lemke, M. *Z. Anorg. Allg. Chem.* **1991**, *605*, 175.

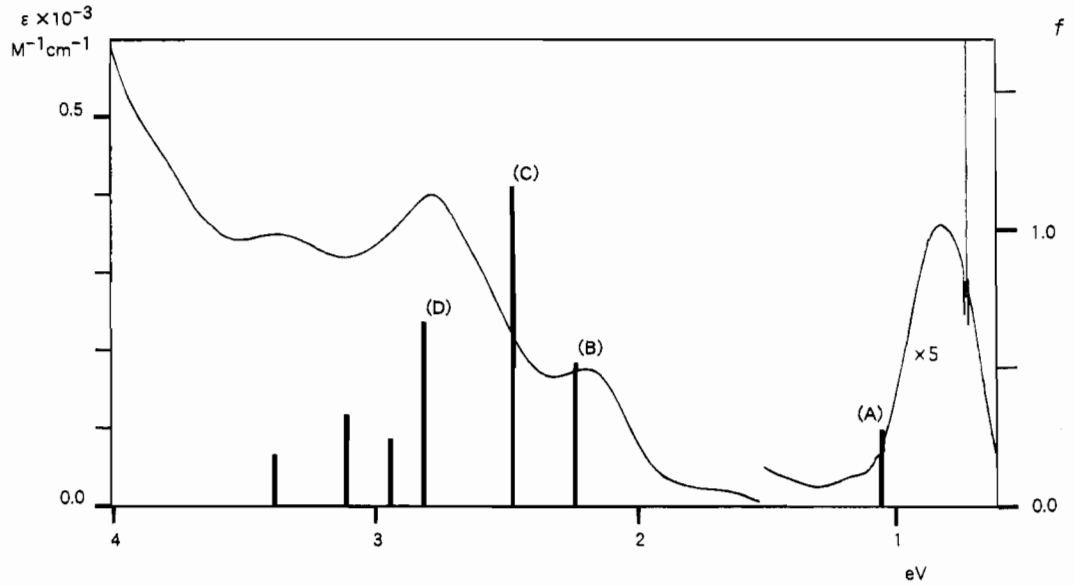

Figure 5. Electronic absorption spectrum of $[Mo_3S_5(PMe_3)_6]$ and calculated oscillation strength of $[Mo_3S_5(PH_3)_6]$. The noise near 0.7 eV is due to solvent ($CHCl_3$).

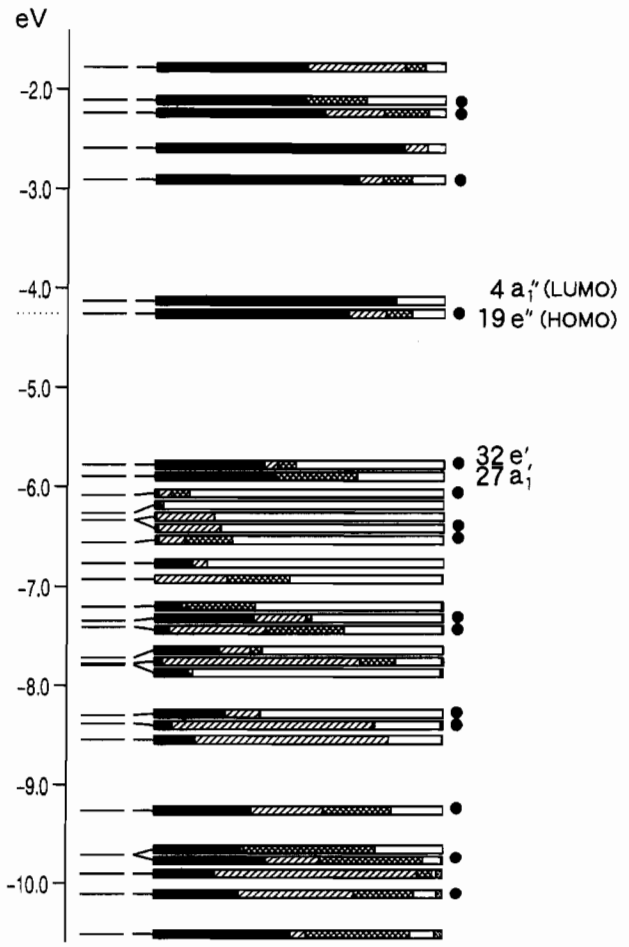

Figure 6. Orbital levels and populations of $[Mo_3S_2Cl_9]^{3-}$ at D_{3h} symmetry. Short horizontal lines show the energies of the levels. The strips show the AO compositions of each MO: black, 4d5s5p(Mo); hatched, 3s3p(μ_2-Cl); cross-hatched, 3s3p(μ_3-S); white, 3s3p(P); dotted, other inner shells. The levels marked with filled circles (●) are degenerate.

composed of three coordination octahedra, but the octahedra share faces in the Mo_3X_5-type clusters while they share edges in the Mo_3X_4 type (Figure 2). Since molybdenum atoms are coordinated octahedrally, the two e_g d orbitals are used for M−L bonding and the three t_{2g} d orbitals are used for metal−metal bonding in both types of clusters.[3,30] The metal−metal bonding and antibonding molecular orbitals constructed from t_{2g} AOs are shown in Figure 7. In an M_3X_5-type cluster, the d_α AOs on three molybdenum atoms make an $a_1'(d_\alpha)$ orbital and an $e'(d_\alpha)$ orbital as shown in Figure 7a. Similarly, the d_β AOs and the d_γ AOs, respectively, make a set of an a-type orbital and an e-type orbital. The energy difference between the a-type orbital and the e-type orbital is determined by the M−M interaction. The $a_1'(d_\alpha)$ and $e'(d_\beta)$ orbitals are stabilized by the M−M σ bonding interaction. However, the orbitals derived from d_γ AOs do not split much because the interaction of the d_γ AOs is π type and weak. As shown in Figure 7b, the splitting pattern of the molecular orbitals of a M_3X_4-type cluster is similar to that of a M_3X_5-type cluster.

When the cluster complex has six skeletal electrons, the three bonding MOs are occupied and the complex has an electron-precise structure. However, when the cluster complex has more skeletal electrons, these electrons occupy the upper MOs e″, a_1'' or a_1, e which are derived from the weakly interacting t_{2g} AOs. The energy of the orbitals constructed from the t_{2g} orbitals are affected not only by the M−M interaction but also by the M−L π interaction, which is mainly between the metal d orbitals and the lone pair orbitals of the ligands. Since the M−M interaction is weak in the MOs constructed from d_γ or $d_{\gamma'}$, the M−L π interaction plays an important role in determining the energy levels of e″, a_1'' and a_1, e. In the case of the Mo_3X_4 type, both metal a_1 and e MOs (especially a_1) are destabilized by the M−L π antibonding interaction. If the interaction is strong, the six-electron system is stabilized; if weak, the a_1' is less destabilized and an eight-electron system is stabilized.[3] In the case of Mo_3X_5, the lone pairs of bridging ligands give a_2'' and e″. Therefore, only the $e''(d_\gamma)$ MO is destabilized by the M−L π antibonding interaction, and the energy of the $a_1''(d_\gamma)$ orbital is not affected by the bridging ligands. In the eight-electron system, if the M−L π antibonding interaction is strong, a_1'' becomes the HOMO and the Mo_3 triangle is equilateral as in $[Mo_3S_5(PMe_3)_6]$. If the interaction is weak, e″ remains the HOMO and the Mo_3 triangle is distorted from equilateral as in $[Mo_3S_2Cl_9]^{3-}$.

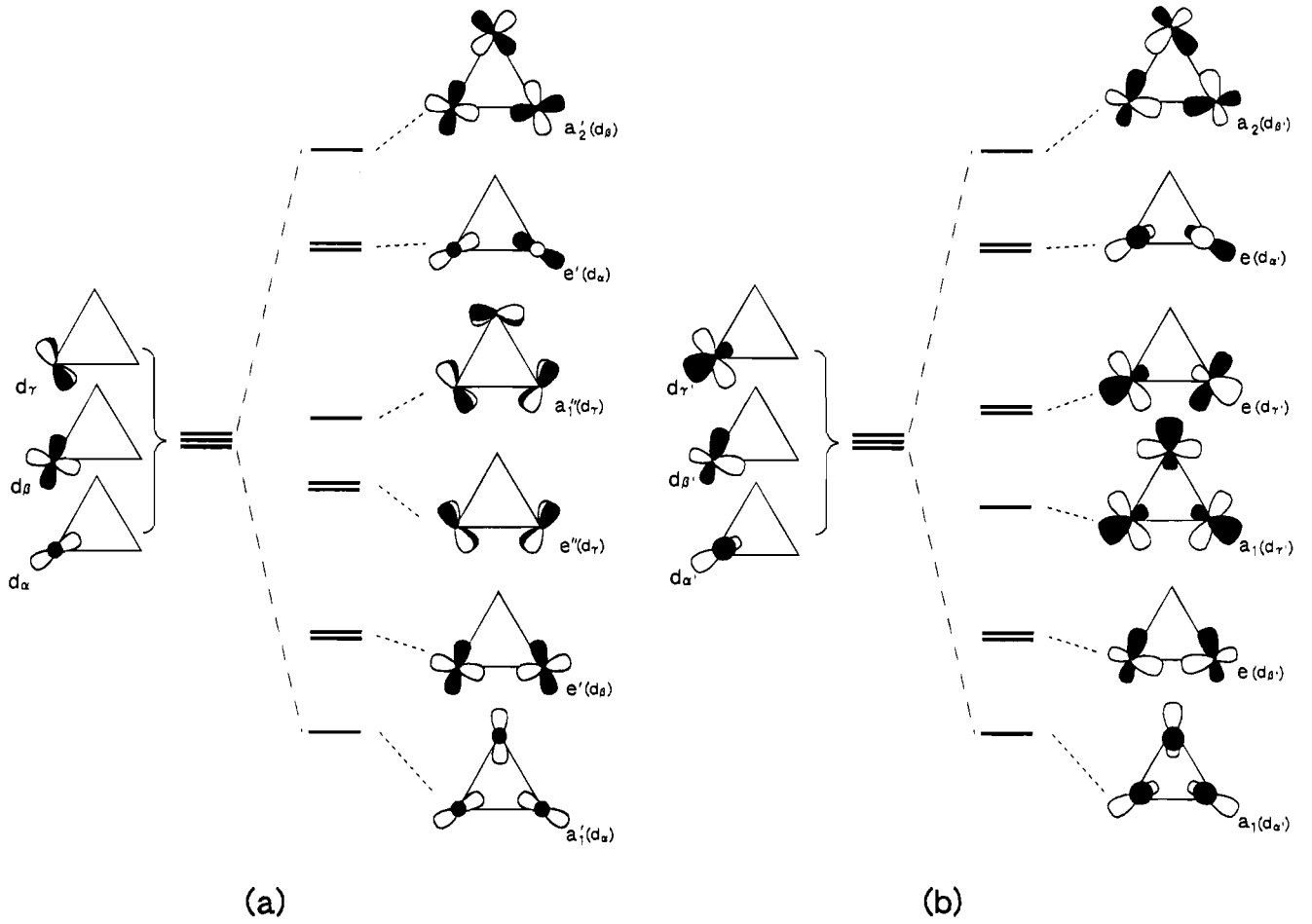

Figure 7. Symmetry-adapted MOs derived from t_{2g} orbitals: (a) for $M_3X_5L_6$; (b) for $M_3X_4L_9$.

Comparison with $[Cr_3S_5(dmpe)_3]$. Arif and co-workers have reported a chromium congener, $[Cr_3S_5(dmpe)_3]$.[32] Though this cluster complex has the same eight skeletal electrons as $[Mo_3S_5(PMe_3)_6]$, the Cr_3 triangle is nearly an isosceles triangle. To explain this deviation from idealized D_{3h} geometry, they have carried out extended Hückel calculations on a model compound $[Cr_3S_5(PH_3)_6]$ at D_{3h} symmetry and proposed that the distortion of the chromium triangle is caused by the second-order Jahn–Teller effect between the HOMO and the LUMO with a rather small HOMO–LUMO gap (0.62 eV). We have carried out DV–Xα calculations on the same chromium D_{3h} model compound and have obtained almost the same result as theirs (HOMO–LUMO gap: 0.66 eV). If the second-order Jahn–Teller effect between the HOMO and the LUMO brings about the distortion, the composition of the HOMO and the LUMO at C_{2v} symmetry should change, and the HOMO–LUMO gap should become larger. However, our calculations on the C_{2v} model compound have shown only slight changes of the composition of the MOs and the HOMO–LUMO gap. The changes of compositions are under 2% and the HOMO–LUMO gap decreases only 0.08 eV for the C_{2v} model. Therefore, it is unlikely that the distortion is caused by the second-order Jahn–Teller effect between the HOMO and the LUMO. We have calculated the D_{3h} model compounds with the Cr–Cr bond lengths in the range 2.50–2.70 Å (the average bond length in $[Cr_3S_5(dmpe)_3]$ is 2.588 Å). Since the HOMO–LUMO gap and the composition of MOs vary little with the change of the bond length (0.62–0.79 eV), the cluster may be easily deformed due to the effect of the packing.

A possible cause of the distortion of the chromium cluster is the effect of crystal packing. The molecules of $[Mo_3S_5(PMe_3)_6]$ are packed in such a manner that the Mo_3 triangles are parallel with each other. The methyl groups of PMe_3 rotate to fit positions to make the molecules approach closer and the overall packing becomes fcc as discussed in the structure section. In contrast, in the crystal of $[Cr_5S_5(dmpe)_3]$, the neighboring Cr_3 triangles are not parallel and the packing is not fcc. The methyl groups in $[Cr_3S_5(dmpe)_3]$ cannot avoid each other because the positions of the methyl groups are determined by the ethylene group which is fixed perpendicularly to the Cr_3 plane. The nonsymmetrical environment around a molecule may cause the deviation from 3-fold symmetry.

Supporting Information Available: Lists of crystallographic data, calculated hydrogen positional parameters, anisotropic thermal parameters, and bond distances and angles (5 pages). Ordering information is given on any current masthead page.

IC940573A

(32) Arif, A. M.; Hefner, J. G.; Jones, R. A.; Albright, T. A.; Kang, S.-K. *J. Am. Chem. Soc.* **1986**, *108*, 1701.